Transverse photothermal beam deflection within a solid

Jonathan D. Spear and Richard E. Russo
Applied Science Division, Lawrence Berkeley Laboratory, Berkeley, California 94720

(Received 4 March 1991; accepted for publication 15 April 1991)

The mirage effect within a transparent solid substrate was used for monitoring optical absorption of a thin film. Refractive index gradients, which accompany thermal gradients below the film-coated surface, cause a probe laser beam to be deflected. The spectrum of copper, deposited onto a piece of clear acrylic, was recorded by this method of photothermal deflection. The influence of thermally induced mechanical stresses can alter the effective value of the thermo-optic coefficient of the solid, dn/dT.

I. INTRODUCTION

The mirage effect as an analytical tool has been established and is generally classified as photothermal deflection spectroscopy (PDS).[1–3] Unlike conventional spectrophotometry, PDS directly measures optical absorption by monitoring thermal gradients. Applications of PDS include absorption studies of flat solid surfaces, such as nonspecular films[4] or electrodes immersed in an aqueous solution.[5] Typically, the sample is in thermal contact with a transparent fluid through which an optical probe beam passes, close to the sample surface. Excitation radiation is transmitted through the fluid, and is incident on the sample. Deflections of the probe beam are monitored and can be correlated with optical absorption. PDS can be preferable to standard spectral reflectance techniques when the sample is light scattering, or is very weakly absorbing (such as a monolayer or submonolayer film upon a dielectric surface). Also, there are special cases for which optical probe beam deflection can be performed *in situ* for observing processes as they occur. For example, beam deflection is currently being investigated as a technique for monitoring thermal gradients and shock waves that result from laser heating and laser damage.[6]

If a sample is thermally thin and is mounted upon a transparent solid substrate through which an optical probe beam passes, we show that the mirage effect can occur below the surface within the solid substrate, rather than above the surface within the fluid. This arrangement might be suitable not only for spectroscopic absorption studies, but also for monitoring other thermal processes. We are particularly interested in applying such a technique to study thermal reactions during laser processing of thin films. For example, if a laser ablates or vaporizes a thin-film target that has been deposited on a transparent substrate, the mirage effect might be used for measuring temperature changes at the surface of the film. Conversely, if a pulsed laser is used to ablate or vaporize[7] a target material for depositing a film of that material onto a transparent substrate, the mirage effect within the substrate could measure the heat produced at the film surface during the deposition process. Although some of these processes can be monitored by beam deflection techniques in the fluid medium outside the sample,[8,9] results are influenced by material ejected from or flowing towards the surface. These influences can be eliminated if the beam deflection occurs behind the sample. This work discusses the theoretically expected behavior of the mirage effect with the probe beam propagating through a transparent solid and, with a simplified experiment using low excitation power, demonstrates the applicability of this method to quantitative analysis of solid films.

II. THEORETICAL

A. Temperature distribution in the solid

Consider the arrangement of Fig. 1, in which an opaque sample film is heated by a modulated source of excitation radiation with an intensity ($W\,cm^{-2}$) equal to $I(t)$. As this radiation is absorbed by the sample, heat is produced, and diffuses away from the surface into a transparent substrate to which the sample is attached. An optical probe laser beam of finite width propagates along the z-axis just below the surface and is deflected by refractive index gradients within the substrate. The surface as shown is circularly concave rather than perfectly flat. The primary reason for incorporating this concavity into the design is to allow the probe beam to pass very near the surface without being obstructed by physical imperfections, such as rounded edges or chips, that might exist in the upper right- and left-hand corners of the substrate. Also, when a flat sample is used, the plane of the sample must be aligned precisely parallel to the path of the probe beam, or else the experimental signal will be strongly affected by slight rotations about the y-axis. The circular curvature in design is beneficial in that the geometry of the region where the sample surface is closest to the axis of the probe beam and contributes most strongly to the mirage effect is insensitive to such rotations. Therefore, the theoretical model that incorporates a curved design should show more reproducible agreement with experiment than the model of a flat sample.

In order to correlate the deflection signal to processes occurring at the surface, it is necessary to determine the temperature distribution T in the transparent solid as a function of position and time. One way of characterizing a system that responds linearly to a given input is to determine the response of the system as a function of time for the case of excitation by an instantaneous impulse function. Then the response of the system to any arbitrary

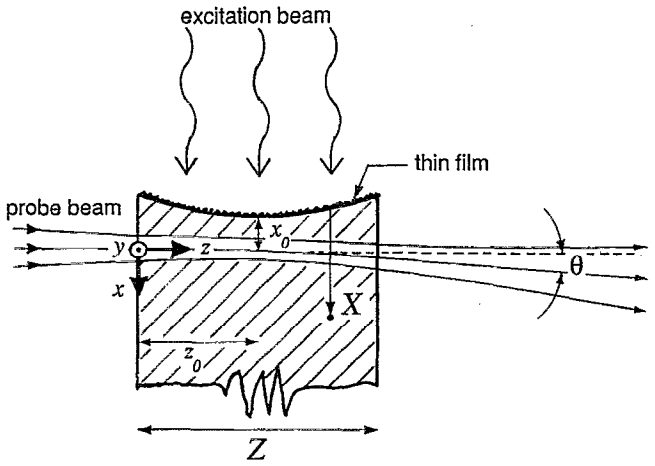

FIG. 1. Geometry of the mirage effect within a transparent solid.

excitation can be determined by integrating over the previous history of excitation. Another method, which we will use, is to solve for the response of the system to an excitation that is sinusoidally varying in time, so that the response of the system can be determined generally by Fourier analysis. We specify several conditions that will be applicable to our particular experimental configuration. The excitation radiation is uniformly incident upon the sample and is temporally square wave modulated such that its intensity has a harmonic component given by $I(t)=I_0\cos(\omega t)$ at the fundamental modulation frequency ω. The sample has absorptance A and converts all absorbed radiation into heat. All heat diffuses into the solid medium by conduction. We also specify that the thickness of the sample is much less than one thermal diffusion length of the sample material. This means that the temperature of the exposed surface of the film is essentially the same as the temperature at the interface between the film and the substrate, and that it is permissible to neglect the heat capacity and thermal conductivity of the sample. A simple thermal diffusion model[3,10] is applicable, using a single dimension X, which we define as the vertical distance below the sample surface. The location specified by $X=0$ corresponds to the boundary between the transparent solid and the sample film, whose actual x-coordinate is a function of z due to the curvature of the surface. Because heat diffusing into the solid originates from this boundary, X more conveniently specifies the temperature within the solid than does x. Such a one-dimensional approximation can be justified when the radius of curvature of the sample surface and the linear dimensions of the heated surface area are much greater than the thermal diffusion length within the transparent solid. Within the transparent solid, the one-dimensional thermal diffusion equation is

$$\frac{d^2T}{dX^2}-\frac{1}{\alpha_{\rm th}}\frac{dT}{dt}=0, \tag{1}$$

where $\alpha_{\rm th}=\kappa/C_p\rho$ is the thermal diffusivity ($\rm cm^2\,s^{-1}$) of the solid. C_p is the heat capacity ($\rm J\,g^{-1}\,K^{-1}$), ρ is the density ($\rm g\,cm^{-3}$), and κ is the thermal conductivity ($\rm W\,cm^{-1}\,K^{-1}$). The boundary condition at the surface of the solid, where $X=0$, can be expressed as a balance of the absorbed power, which is equal to the instantaneous heat flux into the solid:

$$A\ I(t)=-\kappa\left(\frac{dT}{dX}\right)\Big|_{X=0}. \tag{2}$$

Another boundary condition is that the temperature gradient approaches zero as $X\to\infty$. In our analysis, we are concerned only with the time-dependent component of the temperature. The solution to Eqs. (1) and (2) can be expressed compactly by the use of a complex valued function, φ, whose real part represents the actual temperature in the solid:[10]

$$\varphi(X,t)=\frac{A\ I_0}{\kappa\sigma_{\rm th}}\exp(-\sigma_{\rm th}X+i\omega t), \tag{3}$$

where $\sigma_{\rm th}=(1+i)/\mu$, and $\mu=\sqrt{2\alpha_{\rm th}/\omega}$ is the thermal diffusion length (cm). This equation describes a thermal wave whose amplitude decays exponentially from the surface. The gradient of the temperature, as taken from Eq. (3) is

$$\frac{d\varphi(X,t)}{dX}=\frac{-A\ I_0}{\kappa}\exp(-\sigma_{\rm th}X+i\omega t). \tag{4}$$

Equation (4) also describes an exponentially decaying wave for the thermal gradient, dT/dX. The amplitude of this wave is given by the magnitude of φ, and its phase at any value of X is given by the corresponding phase of φ in the complex plane.

B. Refractive index gradients

When the mirage effect occurs within a liquid, it is customary to link refractive index gradients directly to thermal gradients via a material parameter, dn/dT:

$$\nabla n=\frac{dn}{dT}\nabla T. \tag{5}$$

For most fluids, the primary mechanism contributing to dn/dT is thermal expansion of the medium. We have shown[11] that a theoretical value for this parameter is

$$\frac{dn}{dT}=\frac{-\beta}{6n}(n^2-1)(n^2+2), \tag{6}$$

where β is the volumetric thermal expansion coefficient ($\rm K^{-1}$). The underlying assumption of the above equation is that refractive index changes in the fluid material directly result from changes in density. This implies that the fluid material should obey the Lorentz–Lorenz equation. For our experiment, we have selected acrylic, a solid material which has been shown to exhibit this property.[12] When an isotropic solid material is uniformly heated, its volumetric thermal expansion coefficient is equivalent to 3α, where α is the linear thermal expansion coefficient. This equivalence is applicable only for situations in which the solid is allowed to expand freely, in the absence of mechanical stresses. However, thermally induced stresses will always exist when a solid is locally heated, and will

vary depending upon the specific geometry and the boundary conditions of the experiment. Therefore, it becomes necessary to determine the state of volumetric expansion within the solid for the experiment. In our analysis we will assume that the mechanical stresses and expansion of the material do not significantly affect the validity of the thermal diffusion Eq. (1). Then we will derive an "effective" volumetric thermal expansion coefficient, so that an effective value for dn/dT can be calculated and substituted into Eq. (5).

Let us consider the state of our solid material in Fig. 1, which for our demonstrative experiment contains thermal gradients only in the x direction. The film thickness is much less than the thickness of the transparent solid, so we can assume that the mechanical properties of the film material do not contribute to the overall mechanical properties of the film-substrate combination. Also, the region in which thermal gradients exist (approximately one thermal diffusion length) is much less than the thickness of the solid. Therefore, the unheated bulk portion of the solid will constrain the heated layer near the top surface, preventing it from freely expanding thermally along the y and z directions. We describe this effect using thermal tensile stresses, T_y and T_z (N/m^2). Compressive mechanical stress is considered to be negative, and tensile stress is considered to be positive. Because the medium is free to expand in the x direction, no vertical tensile stress exists ($T_x = 0$). Also, because the surface of the sample is uniformly heated and considered to be semi-infinite in extent, a symmetry argument gives that no shear stresses exist. Let us suppose that the material near the surface is heated so that its temperature is changed by an amount ΔT. Following a notation consistent with standard descriptions of mechanical elasticity,[13] and adding the mechanism of thermal expansion into our analysis, we define the following parameters:

e_i=strain in direction i, $i \in \{x,y,z\}$,

E=Young's modulus(N/m^2),

σ=Poisson's ratio.

The component of elongation, or strain, in the x direction due only to heating is given by the linear thermal expansion coefficient:

$$(e_x)_{\text{thermal}} = \alpha \Delta T. \tag{7}$$

And the component of strain in the x direction due only to mechanical stresses can be calculated from Poisson's ratio and Young's modulus:

$$(e_x)_{\text{mechanical}} = \frac{T_x - \sigma(T_y + T_z)}{E}. \tag{8}$$

By superposing these two mechanisms, we obtain an expression for the overall strain in the x direction:

$$e_x = (e_x)_{\text{thermal}} + (e_x)_{\text{mechanical}} = \alpha \Delta T + \frac{T_x - \sigma(T_y + T_z)}{E}. \tag{9}$$

Similar expressions can be written for e_y and e_z:

$$e_y = \alpha \Delta T + \frac{T_y - \sigma(T_x + T_z)}{E}, \tag{10}$$

$$e_z = \alpha \Delta T + \frac{T_z - \sigma(T_x + T_y)}{E}. \tag{11}$$

Now, the boundary conditions are that $e_y = e_z = 0$, and also that $T_x = 0$. Substituting these values into Eqs. (10) and (11) allows us to solve for the thermal stresses:

$$T_y = T_z = \frac{-\alpha E \Delta T}{(1-\sigma)}. \tag{12}$$

And substitution into Eq. (9) gives

$$e_x = \frac{\alpha}{1-\sigma} \Delta T. \tag{13}$$

It is now possible for us to define an effective volumetric thermal expansion coefficient, $\beta_{\text{effective}}$. Because there is no expansion in the y and z directions, $\beta_{\text{effective}}$ is simply the strain in the x direction e_x divided by the change in temperature ΔT:

$$\beta_{\text{effective}} = \frac{\alpha}{1-\sigma}. \tag{14}$$

This result can be substituted into Eq. (6), to obtain an effective value for the material parameter dn/dT:

$$\left(\frac{dn}{dT}\right)_{\text{effective}} = -\frac{\alpha}{(1-\sigma)6n}(n^2-1)(n^2+2). \tag{15}$$

Poisson's ratio generally falls within the range of $\{0 \leqslant \sigma \leqslant 1/2\}$.[13] Therefore $\alpha \leqslant \beta_{\text{effective}} \leqslant 2\alpha$. When dn/dT is measured for a solid material that is heated uniformly, thermal stresses are absent, and $\beta = 3\alpha$. This relation tells us that, in our PDS experiment, $(dn/dT)_{\text{effective}}$ will be reduced to a value that is between 1/3 and 2/3 the measured value for dn/dT.

Although our analytical treatment for determining an effective value of dn/dT is for a simplified case of 1-D heating, it shows some of the basic principles that are applicable to more complex situations. We have assumed that the transparent material is isotropic so that α and σ are the same in all three dimensions. However, Eqs. (7)–(11) can also be written and easily solved for nonisotropic materials as well. If, unlike our case, the surface of the sample is not uniformly heated, then the problem of determining the 3-D temperature distribution and the state of thermal expansion throughout the solid generally becomes more difficult. For example, if a focused laser beam heats the surface of a sample, the locally heated region of the solid has more freedom to expand in the y and z directions than in the uniformly heated case. Therefore, $\beta_{\text{effective}}$ is increased slightly. The temperature distribution within a solid excited by a pulsed laser beam has been considered previously,[1] and a rigorous mathematical treatment of thermal expansion can be found in Ref. 14. Also, it should be noted that dn/dT in many materials, glass for example, is attributable mostly to thermal dependence of electronic polariz-

ability at constant volume rather than thermal expansion of the medium.[15] In this case, refractive index changes due to other such mechanisms can be considered separately and then added to the refractive index changes due to thermal expansion.

C. Propagation of probe beam

For determining the angle of deflection of the probe beam θ, a simple method is to model the beam as a single ray of light with infinitesimal diameter.[1-3] The deflection (in radians) of such a ray, propagating through a medium with small refractive index gradients perpendicular to the direction of propagation z is given by:

$$\theta = \int \frac{\nabla n}{n} dz, \tag{16}$$

where the integration is taken over the path through which the beam passes. When the refractive index gradients are not constant over the finite diameter of the probe beam, a preferred method is to treat the beam as a cluster of rays.[11,16,17] In such an analysis the overall deflection is considered to be an intensity-weighted average of the deflection of individual rays. Typically, the probe beam will exhibit Gaussian spatial properties so that I_p, its intensity (W cm^{-2}), will be given by:[18]

$$I_p(x,y) = \frac{P\pi w^2}{2} \exp\left(\frac{-2(x^2+y^2)}{w^2} \right), \tag{17}$$

where P is the power (W) contained in the beam, and w is the beam radius (cm), specified to be centered at the origin of the x-y plane. As the beam propagates along the z-axis, w contracts and expands in the form of a hyperbola:

$$w^2(z) = w_0^2 \left[1 + \left(\frac{\lambda (z - z_0)}{\pi w_0^2 n} \right)^2 \right], \tag{18}$$

where w_0 is the beam waist radius, and z_0 defines the location of the waist. An intensity-weighted average deflection can be calculated by integration over the volume through which the probe beam passes:

$$\theta = \int_0^Z \frac{\int_{-\infty}^{\infty} dy \int_{-x_0}^{\infty} \frac{\nabla n}{n} \frac{P\pi w^2}{2} \exp\left(\frac{-2(x^2+y^2)}{w^2} \right) dx}{\int_{-\infty}^{\infty} dy \int_{-x_0}^{\infty} \frac{P\pi w^2}{2} \exp\left(\frac{-2(x^2+y^2)}{w^2} \right) dx} dz. \tag{19}$$

The numerator within the integral over the z direction in Eq. (19) represents a 2-D integration over each cross section of the beam of the refractive index gradients weighted by the intensity of the beam. The denominator within the integral normalizes the result with respect to the total power of the beam at each cross section. Note that the lower limit of integration in the x direction is set at $-x_0$ rather than $-\infty$, because it is assumed that optical rays above the line at $x = -x_0$ are blocked by the curved surface of the sample and do not affect the measured deflection of the beam (see Fig. 1). Within the integrals, w is explicitly given as a function of z from Eq. (18). ∇n is specified as a function of X from Eqs. (4), (5), and (15). A transformation for the variable X in terms of the coordinates x and z can be determined from the geometry of the experiment, specifically from R, the radius of curvature of the surface, and x_0, the vertical offset of the probe beam. We have chosen to locate the beam waist in the middle of the sample. Therefore, at the center of the beam waist ($x = 0, z = z_0$), X is equal to x_0. For our experiment, X is described by the equation for a semi-circle in the x-z plane:

$$X = x + x_0 + R - \sqrt{R^2 - (z - z_0)^2}. \tag{20}$$

Equation (19) can be simplified. First, it is possible to factor out and eliminate the $(P\pi w^2/2)$ term from both the numerator and the denominator. Also, because ∇n is not dependent on y, it is permissible to extract the factor $\exp(-2y^2/w^2)$ and integrate separately over y. When these simplifications are performed, Eq. (19) becomes:

$$\theta = \int_0^Z \frac{1}{n} \frac{\int_{-x_0}^{\infty} \nabla n \exp(-2x^2/w^2) dx}{\int_{-x_0}^{\infty} \exp(-2x^2/w^2) dx} dz. \tag{21}$$

The integral over the x dimension within the denominator can also be rewritten as an error function. Here we have assumed that refractive index gradients can exist in the region between the two planes defined by $(z = 0)$ and $(z = Z)$. Equation (21) as written will give the average deflection angle of the probe beam just before it exits the solid medium. In a practical situation, the device that physically measures this deflection angle is usually an optical position sensor placed in air ($n \approx 1$) at some distance from the sample. In order to determine the angle that will be observed experimentally, one can apply Snell's law of refraction to the plane of the solid where the beam exits, at $(z = Z)$, by removing the $1/n$ term from Eq. (21).

III. EXPERIMENT

A. Apparatus

To demonstrate the feasibility of probing the mirage effect within a transparent solid medium, we assembled the apparatus shown in Fig. 2. A 108-W tungsten ribbon filament lamp was focused by a glass lens L_3 into a 0.25 m, f3.5 Jarrell–Ash Ebert monochromator, to provide a tunable excitation light source. A mechanical chopper (Stanford Research Systems model SR 540) located at the exit slit of the monochromator modulated the excitation light, which was focused by a 57 mm, f1.4 camera lens L_4 onto the surface of the sample. The focused image of the exit slit had a width of 0.10 cm in the y direction. The length of the slit image in the z direction was 0.42 cm and determined the value of Z to be used in the integral of Eq. (21). A He-Ne laser (Uniphase model 1303P) with an output wavelength of 632.8 nm served as the optical probe beam. This beam was first expanded by a concave lens L_1 with a focal length of -5 cm, and then focused by a convex lens L_2 with a focal length of 6.3 cm. The separation between the two lenses was 8 cm. This lens arrangement produced a beam waist radius of $w_0 = 30 \pm 5$ μm, as measured by a photodiode mounted behind a movable pinhole. The de-

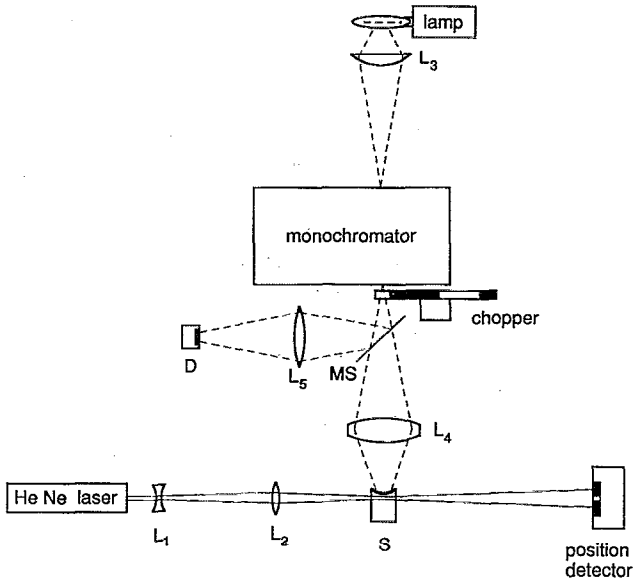

FIG. 2. Schematic diagram of experimental apparatus.

flection of the beam was monitored by a continuous single axis dual cathode photodiode (United Detector Technologies model LSC-5D), which was placed 25 cm beyond the beam waist. A UDT model 301-DIV differential amplifier monitored the photocurrents from the position detector and produced a signal proportional to the angle of deflection. The output of the position sensor amplifier was fed into an EG&G ORTEC model Ortholoc-SC9505 lock-in amplifier, which, using the timing signal from the chopper as a frequency reference, provided a measure of the amplitude of the deflection. A thin glass microscope slide MS, diagonally placed between the chopper and the camera lens, acted as a beam splitter to reflect a fraction of the excitation light through another lens L_5 and onto a radiometric photodiode D (UDT model PIN-10DF). For normalization of the deflection signal with respect to the excitation light intensity, the photocurrent from this detector was amplified by a UDT model 101A transimpedance amplifier and measured by a second lock-in amplifier (PAR model 126). An SRS model SR235 analog processor divided the electrical output of the first lock-in by that of the second to provide the normalized photothermal deflection amplitude. The sample S consisted of an opaque copper film upon a transparent piece of 0.635 cm thick cast acrylic window material (Rohm and Haas brand Plexiglas). The edge of the acrylic was machined with a 1.27-cm radius mill bit to make it concave as in Fig. 1, and the copper was sputtered to a thickness of about 0.2 μm onto this curved edge. No special lapping or polishing preparations were performed on the acrylic surface before the film deposition process. Because the thermal diffusion length in copper is about 0.13 cm at a modulation frequency of 20 Hz, our original assumption that the sample be thermally thin is appropriate. The center of the sample was first positioned along the z axis at the probe beam waist and then was carefully translated in the x direction so that the probe beam could enter and exit the two flat faces of the acrylic without apparent distortion.

The material parameter dn/dT for acrylic has been measured experimentally under conditions of uniform heating and is reported[12] to be $-1.05 \times 10^{-4}\,\mathrm{K}^{-1}$ at a temperature of 20 °C and a wavelength of 632.8 nm. Its coefficient of linear thermal expansion is $\alpha = 6.8 \times 10^{-5}\,\mathrm{K}^{-1}$, and its refractive index is $n = 1.493$. Substitution of these two parameters into Eq. (6) predicts a value for dn/dT of $-1.18 \times 10^{-4}\,\mathrm{K}^{-1}$, which is close to the measured value. Poisson's ratio, as quoted by the manufacturer, is $\sigma = 0.35$. Insertion of this value into Eq. (15) tells us that we should expect to observe a value of $(dn/dT)_{\text{effective}} = -6.0 \times 10^{-5}\,\mathrm{K}^{-1}$, or about half the value measured for dn/dT under uniform heating. Although this effective value is reduced, it is still comparable to that of water and other liquids commonly used for PDS studies. Other relevant material parameters for acrylic are its thermal conductivity $\kappa = 1.88 \times 10^{-3}\,\mathrm{W\,cm^{-1}\,K^{-1}}$, its heat capacity $C_p = 1.47\,\mathrm{J\,g^{-1}\,K^{-1}}$, and its density $\rho = 1.19\,\mathrm{g\,cm^{-3}}$. These values give a thermal diffusion length of about 40 μm at a modulation frequency of 20 Hz. Because the thermal diffusion length in acrylic is much less than the linear dimensions of the excitation beam incident on the sample, our 1-D heating model is appropriate. Also, the product of κ, ρ, and C_p for acrylic is much greater than the product of the corresponding numbers for air. Therefore it is permissible to neglect heat transfer by conduction from the surface of the sample into air, as we have done in Eq. (2).

B. Beam offset

It is difficult to make a direct measurement of x_0, the transverse offset of the probe beam. We attempted to deduce a value for x_0 indirectly by observing the dependence of the deflection signal on the modulation frequency ω. The deflection amplitude generally decreases with increasing modulation frequency. Also, the amount by which the phase of the deflection lags the phase of the excitation source increases with increasing frequency. To observe these trends, we first removed the diffraction grating from its place in the monochromator. This allowed white light to pass directly from the tungsten lamp straight through both slits of the monochromator, so that a large photothermal deflection signal could be obtained, relatively unaffected by noise from air currents or mechanical vibrations of optical components. After fixing the alignment of the sample with respect to the probe beam, we used the first lock-in amplifier to compare the deflection amplitude and phase at three different modulation frequencies: $\omega/2\pi = 11$, 21, and 39 Hz. The ratio of measured deflection amplitudes at the three frequencies was 1:0.49:0.11, respectively. It was also observed that the relative phase of the deflection signal changed by 46° when the modulation frequency was increased from 11 to 21 Hz, and by an additional 64° when the frequency was increased to 39 Hz. To interpret these trends, we computed the theoretical amplitude and phase of the deflection using Eqs. (4), (5), (15), (18), and (21). The results of these calculations are

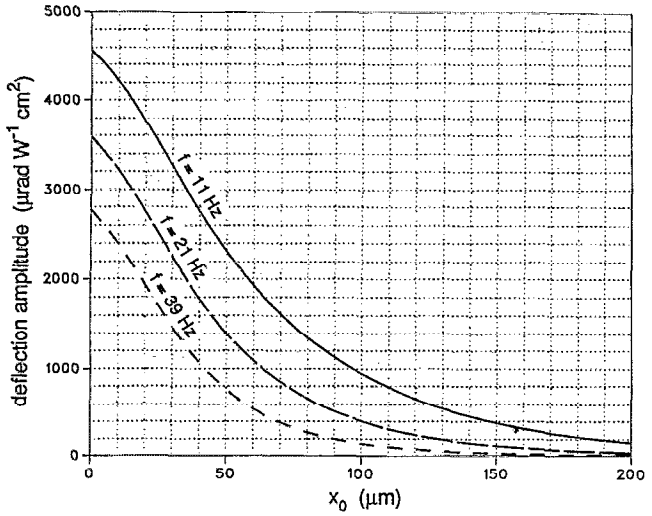

FIG. 3. Theoretical deflection amplitude as a function of beam offset for three different modulation frequencies. Units are normalized with respect to the intensity of absorbed excitation radiation.

shown in Figs. 3 and 4. The integrations of Eq. (21) were numerically evaluated (with the 1/n term removed) by using a simple computer program that approximated each integral as the sum of areas under rectangles. In Fig. 3, the amplitude of the deflection is expressed in units of μrad W^{-1} cm^2, so as to normalize the results with respect to the absorbed excitation power per unit area, which has units of W cm^{-2} and is equal to the product of absorptance and incident intensity. The decrease in signal amplitude with increasing modulation frequency limits the usable bandwidth of the mirage effect, so our arrangement will not be practical for temporal resolution of very fast thermal processes. In Fig. 4, a positive phase lag indicates that there is a time delay between the excitation of the sample and the

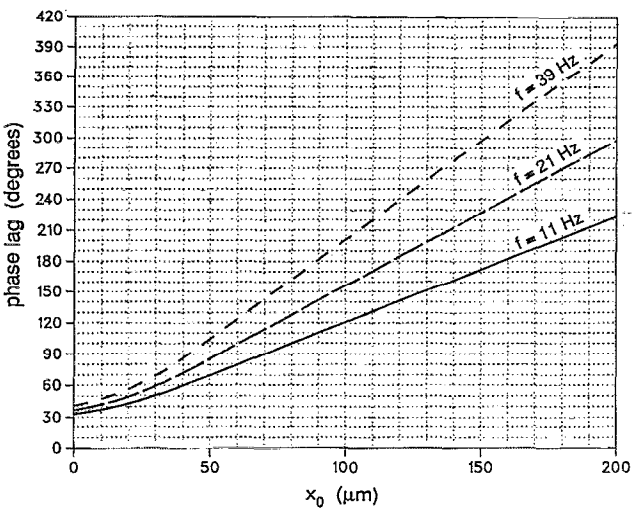

FIG. 4. Theoretical phase lag between photothermal deflection signal and excitation radiation as a function of beam offset for three different modulation frequencies.

subsequent deflection of the beam. From the calculations shown in these figures, we approximated the beam offset x_0 to be 125 μm. At this value of x_0, the theory gives the ratio of deflection amplitudes at 11, 21, and 39 Hz should be 1:0.36:0.10, and the phase lag should increase by 45° between 11 and 21 Hz, and by 57° between 21 and 39 Hz.

C. Calibration of system

Without changing the alignment of the sample, we replaced the grating and set the widths of the slits on the monochromator to 2.2 mm. This adjustment provided an optical bandpass of 9 nm FWHM. The wavelength of excitation light was set at 633 nm, and the modulation frequency was 11 Hz. The electrical amplitude measured by the first lock-in amp was 31 μV, which corresponded in our apparatus to a deflection amplitude of 3.7×10^{-8} rad. At this wavelength, the excitation radiation incident on the sample had a modulated intensity (as monitored by the second lock-in amp) with an amplitude of 4.6×10^{-3} W cm^{-2}. From a separate test using the HeNe laser normally incident on the copper film and a photodiode, we measured the reflectance of the sample to be 0.85 at this wavelength. This measurement implied a value of $A = 0.15$, from which we calibrated the response of the mirage effect with respect to radiation absorbed by the sample to be 54 μrad W^{-1} cm^2. The observed value is an order of magnitude lower than the 600 μrad W^{-1} cm^2 that is predicted with $x_0 = 125$ μm in the theoretical model, whose results are shown in Fig. 3. This discrepancy between theory and experiment in the absolute magnitude of deflection is greater than that found for collinear PDS,[11] which has been shown to agree within a factor of 2. To our knowledge, no previous work in transverse PDS has been published that has compared this experimental calibration of absolute deflection magnitude to the magnitude predicted by theory. In addition to the accumulation of measurement error, a possible cause for the discrepancy that we observe in transverse PDS is that microscopic flaws and roughness in the surface of the acrylic might influence the flow of the thermal wave into the acrylic and thereby reduce the observed amplitude of the deflection. Another possibility is that a portion of the probe beam radiation is reflected off the back surface of the sample onto the position sensor and alters the measured deflection signal. In any case, the experimental calibration of the apparatus seems to be necessary for quantitative measurements.

D. Spectral results

Our technique of probe beam deflection inside an acrylic block responds accurately to changes in the absorptance of the surface film. Copper was chosen because it has a characteristic absorption band edge centered about 570 nm. To record the absorption spectrum of the copper film, the wavelength of the monochromator was scanned at a constant rate of 20 nm/min from 500 to 700 nm, and the normalized photothermal deflection spectrum was recorded on an X-Y plotter (Fig. 5). During this scan, the time constant of the lock-in amplifier was set at 3 s. The

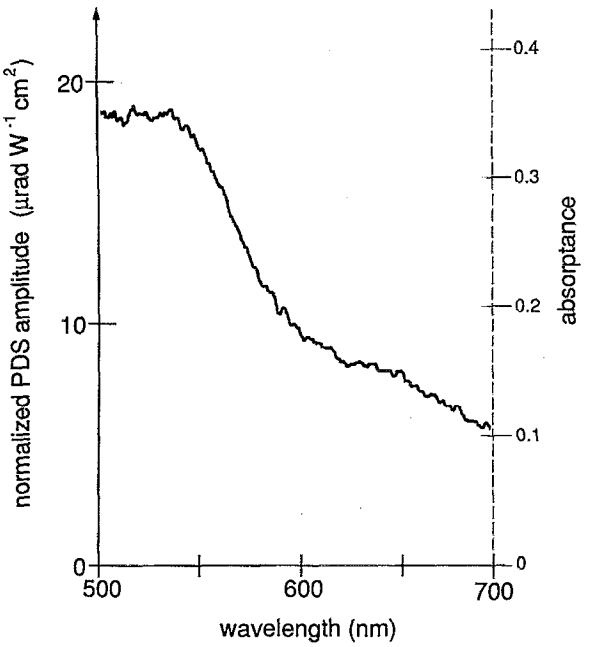

FIG. 5. Normalized photothermal deflection signal amplitude of a copper film as a function of excitation wavelength. A calibrated scale corresponding to the sample absorptance is shown on the right-hand side.

level of irradiance incident on the sample varied during this scan from 1.9×10^{-3} W cm^{-2} at a wavelength of 500 nm to 5.1×10^{-3} W cm^{-2} at a wavelength of 700 nm. The normalized absorption spectrum shows that the absorptance of copper decreases as wavelength is increased, successfully indicating the characteristic reddish color of the metal that can also be observed by spectral reflectance measurements.[19]

IV. DISCUSSION

We have demonstrated a novel application of photothermal deflection spectroscopy within a solid medium. A theoretical model for determining an effective value for dn/dT has been developed for solid materials when thermal expansion is the important mechanism for this parameter. The effect within acrylic has been shown to be strong enough that a low power lamp could be used as the excitation source. If a more powerful excitation source such as a laser is used, this mirage effect should be easier to observe.

Unlike conventional techniques which measure reflectance, quantitative absorptance measurements using transverse PDS require an initial calibration with a standard sample of known absorptance. The absolute accuracy of PDS measurements is affected by the accuracy of this initial calibration. Other practical considerations that factor into the accuracy of PDS include the alignment stability of the system, because the observed deflection amplitude is strongly dependent upon x_0, and ambient temperature changes, which might effect either dn/dT or the other thermal parameters of the deflecting medium. Important noise sources for PDS include beam pointing of the probe laser, mechanical vibrations of optical components, and air currents within the laboratory. Such experimental noise can limit the sensitivity of the technique.

Thanks are due to David Wruck and David Schurig for their helpful comments on the manuscript, and to David Wruck also for his assistance in preparing the sputtered copper sample. This research was supported by the U.S. Department of Energy, Office of Basic Energy Sciences, Division of Chemical Sciences, under Contract No. DE-AC03-76SF00098.

[1] W. B. Jackson, N. M. Amer, A. C. Boccara, and D. Fournier, Appl. Opt. **20**, 1333 (1981).
[2] A. C. Boccara, D. Fournier, and J. Badoz, Appl. Phys. Lett. **36**, 130 (1980).
[3] A. Mandelis, J. Appl. Phys. **54**, 3404 (1983).
[4] B. S. H. Royce, F. Sanchez-Sinencio, R. Goldstein, R. Muratore, R. Williams, and W. M. Yim, J. Electrochem. Soc. **129**, 2393 (1982).
[5] R. E. Russo, F. R. McLarnon, J. D. Spear, and E. J. Cairns, J. Electrochem. Soc. **134**, 2783 (1987).
[6] S. Petzoldt, A. P. Elg, M. Reichling, J. Reif, and E. Matthias, Appl. Phys. Lett. **53**, 2005 (1988).
[7] R. K. Singh and J. Narayan, Phys. Rev. B **41**, 8843 (1990).
[8] J. A. Sell, D. M. Heffelfinger, P. Ventzek, and R. M. Gilgenbach, Appl. Phys. Lett. **55**, 2435 (1989).
[9] C. L. Enloe, R. M. Gilgenbach, and J. S. Meachum, Rev. Sci. Instrum. **58**, 1597 (1987).
[10] A. Rosencwaig and A. Gersho, J. Appl. Phys. **47**, 64 (1976).
[11] J. D. Spear, R. E. Russo, and R. J. Silva, Appl. Opt. **29**, 4225 (1990).
[12] R. M. Waxler, D. Horowitz, and A. Feldman, Appl. Opt. **18**, 101 (1979).
[13] R. A. Beth, in *Handbook of Physics*, edited by E. U. Condon and H. Odishaw (McGraw-Hill, New York, 1959), Part 3, Chap. 5, pp. 3.64–3.77.
[14] W. Nowacki, *Thermoelasticity* (Pergamon, New York, 1986).
[15] R. M. Waxler and G. W. Cleek, J. Res. Natl. Bur. Stand. Sect. A **77**, 755 (1973).
[16] E. Legal Lasalle, F. Lepoutre, and J. P. Roger, J. Appl. Phys. **64**, 1 (1988).
[17] L. C. Aamodt and J. C. Murphy, J. Appl. Phys. **52**, 4903 (1981).
[18] H. Kogelnik and T. Li, Appl. Opt. **5**, 1550 (1966).
[19] F. A. Jenkins and H. E. White, *Fundamentals of Optics*, 3rd ed. (McGraw-Hill, New York, 1957), p. 522.